Ground state energy and width of ^{7}He from ^{8}Li proton knockout

D. H. Denby,[1] P. A. DeYoung,[1] T. Baumann,[2] D. Bazin,[2] E. Breitbach,[3] J. Brown,[4] N. Frank,[2,5,*] A. Gade,[2,5] C. C. Hall,[1] J. Hinnefeld,[6] C. R. Hoffman,[7] R. Howes,[3] R. A. Jenson,[8] B. Luther,[8] S. M. Mosby,[2,5] C. W. Olson,[8] W. A. Peters,[2,5] A. Schiller,[9] A. Spyrou,[2] and M. Thoennessen[2,5]

[1]*Department of Physics, Hope College, Holland, Michigan 49423, USA*
[2]*National Superconducting Cyclotron Laboratory, Michigan State University, East Lansing, Michigan 48824, USA*
[3]*Department of Physics, Marquette University, Milwaukee, Wisconsin 53201, USA*
[4]*Department of Physics, Wabash College, Crawfordsville, Indiana 47933, USA*
[5]*Department of Physics and Astronomy, Michigan State University, East Lansing, Michigan 48824, USA*
[6]*Department of Physics and Astronomy, Indiana University at South Bend, South Bend, Indiana 46634, USA*
[7]*Department of Physics, Florida State University, Tallahassee, Florida 32303, USA*
[8]*Department of Physics, Concordia College, Moorhead, Minnesota 56562, USA*
[9]*Department of Physics and Astronomy, Ohio University, Athens, Ohio 45701, USA*

(Received 16 July 2008; published 13 October 2008)

The ground state energy and width of ^{7}He has been measured with the Modular Neutron Array (MoNA) and superconducting dipole Sweeper magnet experimental setup at the National Superconducting Cyclotron Laboratory. ^{7}He was produced by proton knockout from a secondary ^{8}Li beam. The measured decay energy spectrum is compared to simulations based on Breit-Wigner line shape with an energy-dependent width for the resonant state. The energy of the ground state is found to be 400(10) keV with a full-width at half-maximum of $125(^{+40}_{-15})$ keV.

DOI: 10.1103/PhysRevC.78.044303 PACS number(s): 21.10.Dr, 21.10.Pc, 27.20.+n, 29.30.Hs

I. INTRODUCTION

The neutron-rich nucleus ^{7}He is particle unstable and decays into ^{6}He and a neutron. The properties of the $3/2^{-}$ ^{7}He ground state have been studied extensively [1–30] and the results are summarized in Table I. Although the publication list is long, it is interesting to note that only a few articles report independent measurements of the ground state resonance parameters. Following the initial transfer-reaction measurements by Stokes and Young [1,2] there are only three measurements of the energy [17,20,22] and two of the width [18,26] with a precision better than 50 keV. The continued interest in ^{7}He is motivated by the search for the missing first excited $\frac{1}{2}^{-}$ state. Two recent measurements [20,27] posited evidence of a low-lying $\frac{1}{2}^{-}$ excited state; however, this finding has been disputed by other measurements reported in Refs. [21] and [22].

The previous measurements of ^{7}He listed in Table I have employed 19 different reactions as shown in Fig. 1. Up to now, ^{7}He has not been populated using the proton knockout reaction from ^{8}Li. In the present work, we report our findings for the decay energy and resonance width of the ground state of ^{7}He populated with this reaction. The proton knockout reaction should strongly populate the ground state, but in first order should not populate the $\frac{1}{2}^{-}$ excited state. The measurement was performed at the National Superconducting Cyclotron Laboratory (NSCL) with the Modular Neutron Array (MoNA) [31,32], the high-field superconducting dipole (Sweeper) magnet [33], and associated charged-particle detectors.

II. EXPERIMENTAL PROCEDURE

A ^{8}Li beam of 41 MeV/nucleon was produced at the NSCL by accelerating a primary beam of ^{18}O with the Coupled Cyclotron Facility to 120 MeV/nucleon. The primary beam impinged on a 3526 mg/cm^2 Be A1900 production target and the resulting fragments were separated in flight with the A1900 fragment separator [34]. An 825 mg/cm^2 Al achromatic degrader installed at the dispersive plane of the A1900 enabled the isotopic separation of the secondary ^{8}Li beam. This beam had a magnetic rigidity of 2.4994 Tm and slits in the A1900 were configured to give a momentum acceptance of $\pm 0.4\%$. A 254 μm scintillator located just before the beryllium reaction target served as a timing start detector for measuring neutron and incident beam time-of-flight (TOF). While there was a small amount of contamination in the beam, the results presented here required the proper TOF between the A1900 and the start detector to ensure only events involving incident ^{8}Li were included. The position and direction of each incident particle was tracked with a pair of high-rate cathode readout drift chambers (CRDCs) located upstream of the experiment reaction target. The beam was then focused onto a 192 mg/cm^2^{9}Be reaction target with a superconducting quadrupole triplet lens. Following one-proton knockout, ^{7}He immediately decayed into a ^{6}He and a single neutron.

The neutrons were detected with MoNA [31,32], which was located 8.2 m from the beryllium reaction target and centered about 0° relative to the beam direction. The location of the interaction point of the neutron in MoNA was determined by the particular detector module that registered the neutron (for the vertical position and distance along the beam axis) and by the time difference between the signals from the left and right photomultiplier tube (PMT) of each module for the

*Present address: Physics Department, Illinois Wesleyan University, Bloomington, IL 61701, USA.

TABLE I. Summary of previous measurements of ^{7}He. All resonance energies and widths are given in keV. In most cases Γ represents the FWHM, although it is sometimes not explicitly stated.

Reference	Reaction	Ground state		1st Excited state	
		E_{gs}	Γ	E^*	Γ
[1]	^{7}Li(t, ^{3}He)	420(60)	170(40)	–	–
[2]	^{7}Li(t, ^{3}He)	440(30)	160(30)	–	–
[3]	^{7}Li(n, p)	∼400[a]	<200	–	–
[4]	^{9}Be(^{6}Li, ^{8}B)	Observed		No resonances	⩽10 MeV
[5]	^{9}Be(^{6}Li, ^{8}B)	Observed		No resonances	⩽10 MeV
[5]	^{7}Li(^{7}Li, ^{7}Be)	Observed		No resonances	⩽10 MeV
[6]	^{7}Li(π^-, γ)	340(80)[b]		No resonances	⩽15 MeV
[7,8]	^{9}Be(^{14}C, ^{16}O)[c]	500(300)	150(50)	2900(300)[d]	
[9]	^{18}O fragm.	450[e]	160[e]	–	–
[10,11]	^{6}Li(^{14}C, ^{13}N)	Observed[f]		No resonances	⩽10 MeV
[12]	^{18}O fragm.	450[e]	160[e]	–	–
[13][g]	^{9}Be(^{15}N, ^{17}F)	Observed[f]		3160(50)	1500(200)
[14,15]	p(^{8}He, d)	440[e]	160[e]	2900(300)	2200(300)
[16]	d(^{6}He, p)	Observed		No resonances	⩽8 MeV
[17]	^{11,12}Be fragm.	450(20)	160[e]	–	–
[18]	^{9}Be(^{15}N, ^{17}F)	440[h]	140(20)	2950(100)	1900(200)[i]
[19][j]	^{8}He n-knockout	440[e]		800(200)	1000(200)
[20]	^{8}He n-knockout	430(20)	150(80)	600(100)	750(80)
[21,22]	p(^{6}He, n) IAS	410(30)		(∼2700)	(∼8000)
[23]	d(^{6}He, p)	Observed[k]		2600	∼2000
[24]	^{7}Li(^{7}Li, ^{7}Be)	Observed[f]		∼2900	
[25,26]	^{7}Li(d, 2p)	446	183(22)	1450^{+70}_{-50}	2000^{+1000}_{-1100}
[27]	p(^{8}He, d)	360(50)	170(50)	900(500)	1000(900)
[28]	Nuclear data eval.	445(30)	150(20)	2920(90)	1990(170)
[29,30]	Atomic mass eval.	435(17)	160(30)[l]		

[a]Derived from a proton peak "near" 3.8 MeV.
[b]Derived from $E_\gamma = 126.73(8)$ MeV. $E_\gamma = 126.6$ MeV from Table 6 of Ref. [6] yields $E_{gs} = 470$ keV.
[c]Ref. [8] also observed the ground state in the reactions ^{7}Li(^{11}B, ^{11}C), ^{9}Be(^{11}B, ^{13}N), and ^{9}Be(^{9}Be, ^{11}C).
[d]Ref. [7] quotes 3500(500) keV and 2000(500) keV for the energy and width of the excited state, respectively.
[e]Consistent with data, no fit performed.
[f]Resonance parameters taken from literature.
[g]Preliminary analysis, data also published in Ref. [18].
[h]Taken from literature, no absolute mass measurement was performed.
[i]An uncertainty of 300 keV is quoted in the abstract.
[j]Preliminary analysis, data also published in Ref. [20].
[k]Resonance located at the reaction $Q_g = -2.669$ MeV taken from literature.
[l]Converted from $T_{1/2} = 2.9(5) \times 10^{-21}$.

horizontal location. The neutron TOF was determined from the average of the times recorded for the two PMTs at the ends of the module. The zero point for this time scale was determined from the known distance between the reaction target and MoNA and the measured flight time for γ rays produced in the reaction target. The ^{6}He were deflected with the Sweeper magnet [33] into two CRDCs, separated by 1 m, that measured the trajectories of the particles. The ^{6}He then impinged on a set of thin (5 mm) and thick (15 cm) plastic scintillators, giving energy loss and total energy, which unambiguously identified the ^{6}He fragments. The position calibrations (in particular the drift time, which gives the vertical position) of the CRDCs were checked regularly throughout the run [35]. A measured magnetic field map for the Sweeper was used as the input to the ion optics code COSY [36] to determine a transformation matrix that converts the positions and angles of the trajectory into direction and energy of the ^{6}He at the reaction target. While the standard transformation matrix from COSY is based on an assumption that all the incident ions impact the reaction target with no spread in the dispersive plane (identically at $x = 0$), the transformation matrix for this work was parametrized to include the measured position of each incident ion at the reaction target [37]. The energy was also corrected for energy loss of the ^{6}He through half the beryllium reaction target, 0.85 MeV/u. The depth of the interaction point in the reaction target is not known, so the ^{6}He energy was corrected by assuming all the interactions took place in the center of the reaction target.

The hardware trigger for the experiment required a charged particle to register in the thin scintillator within 400 ns of a

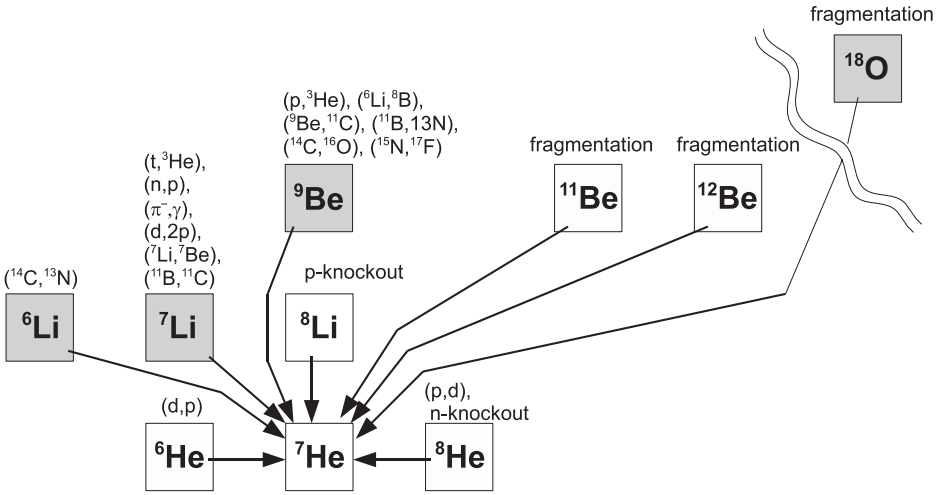

FIG. 1. Summary of reactions resulting in ^{7}He. A small section of the chart of the nuclei with only the nuclei of interest is shown. Grey denotes stable nuclei that were used as targets (^{6,7}Li and ^{9}Be) or beam (^{18}O). Open squares near ^{7}He denote unstable isotopes used as beams. The thick borders indicate the beam and resulting unstable isotope from this work.

signal from any module in MoNA. Further restrictions were applied during offline analysis.

The neutron energy and direction are known as are the ^{6}He energy and direction. With this information, the four-vector of the ^{7}He is calculated in the laboratory frame with

$$\begin{bmatrix} E_{^7\mathrm{He}} \\ \vec{p}_{^7\mathrm{He}} \end{bmatrix} = \begin{bmatrix} E_{^6\mathrm{He}} \\ \vec{p}_{^6\mathrm{He}} \end{bmatrix} + \begin{bmatrix} E_{\mathrm{n}} \\ \vec{p}_{\mathrm{n}} \end{bmatrix} \tag{1}$$

from the laboratory frame four-vectors for the ^{6}He and the neutron event by event. The invariant mass is found from

$$m^2_{^7\mathrm{He}} = m^2_{^6\mathrm{He}} + m^2_{\mathrm{n}} + 2(E_{^6\mathrm{He}}E_{\mathrm{n}} - p_{^6\mathrm{He}}p_{\mathrm{n}}\cos\theta), \tag{2}$$

which is the result of the square of each side of Eq. (1). The known mass of the neutron and ^{6}He are then subtracted from the invariant mass of the system to obtain the decay energy spectrum of ^{7}He.

$$E_{\mathrm{decay}} = m_{^7\mathrm{He}} - m_{^6\mathrm{He}} - m_{\mathrm{n}}. \tag{3}$$

In Eqs. (1)–(3), m is the rest mass of the respective particle, E is the total energy, $\vec{p}$ is the vector three-momentum, p is the magnitude of the momentum, and θ is the angle between the neutron momentum and the fragment momentum in the laboratory frame.

III. SIMULATION

The decay energy spectrum obtained as described above contains a peak (or multiple peaks if multiple states exist and are populated) whose shape is related to the energy and width of the unbound state. The spectral shape is affected by many experimental factors such as the detector resolutions and acceptances so that the energy and width cannot be directly extracted from the measured decay energy spectrum. Rather than trying to correct the measured spectrum, a simulation package was developed to produce data that incorporate information about the sizes, locations, acceptances, and resolutions of the detectors; beam properties; and the properties of the decaying state. The simulated events were then analyzed and sorted in the same way as the experimental data.

The simulation included a parametrization of the reaction mechanism to produce ^{7}He in the beryllium reaction target. The peaks of the velocity (or energy/nucleon) distributions of the neutrons (see Fig. 2) and the fragments (see Fig. 3) are higher than those of the beam energy of the incoming ^{8}Li fragments after taking into account the energy losses in the reaction target. In the fragmentation models based on the Glauber description the outgoing fragment velocity is typically equal or smaller than the incoming projectile velocity [38]. Thus we considered the possibility that the two-body reaction ^{9}Be(^{8}Li,^{7}He)^{10}B could contribute. The pickup of a proton by the ^{9}Be reaction target, which is bound by more than 12 MeV, can occur at beam energies of 40 MeV/nucleon. Thus, sizable contributions of the two-body reaction mechanism are not unreasonable. The relative contribution of each of the two reaction mechanisms was determined by reproducing the neutron energy, fragment energy, and opening angle distributions. In addition, a Q value of -8.0 MeV with a width of 0.275 MeV for the two-body reaction was necessary to fit these spectra.

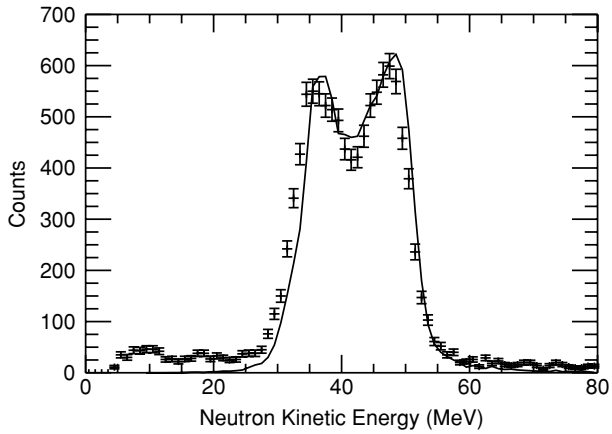

FIG. 2. The measured neutron kinetic energy spectrum. The dip at 40 MeV is due to decays in the ^{7}He center-of-mass frame that emit the neutron and fragment sideways away from the laboratory velocity resulting in laboratory angles greater than the acceptance of MoNA. The solid line is the result of simulation.

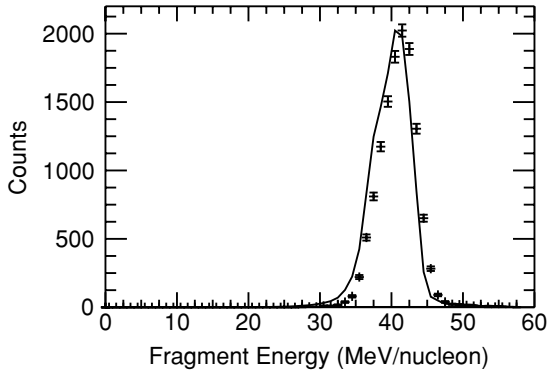

FIG. 3. The measured ^{6}He kinetic energy spectrum. The solid line is the result of simulation.

The ^{7}He ground state decay energy distribution is parametrized as a Breit-Wigner line shape with an energy-dependent width. The width depends on the partial width of the resonance, the angular momentum of the resonant state, and its energy. With only a single decay channel, the partial and total widths are the same and given by the expression $\Gamma_{\rm tot} = 2\gamma^2 P_l(E_r)$, where γ^2 is the reduced width and $P_l(E_r)$ is the penetrability function. The penetrability carries the energy and angular momentum dependence of the total width, as the reduced width γ^2 is constant and holds the nuclear structure information. Specific details of this line shape can be found in Ref. [39]. The total width in this relationship is not equal to the full-width at half-maximum (FWHM) of the distribution. The latter is typically quoted in the literature.

Finally, to determine the resonance energy and width, a series of simulations was carried out where the energy, width, reaction-mechanism ratio, and normalization were varied to minimize the reduced χ^2 for the decay energy spectrum. The difference between data and simulation for the neutron kinetic energy distribution, the ^{6}He energy spectrum, and the opening angle spread were not included in the χ^2 calculation but were used to constrain the range of values as the four simulation variables were adjusted. The estimated uncertainties for the energy and width are based on the range of values that resulted in reasonable overall agreement in all the spectra while allowing the reduced χ^2 to increase by one. It was observed that the resonance energy is quite insensitive to most of the possible systematic errors. Tests were done where MoNA was artificially shifted to the side, the time offset for the neutron TOF as shifted, and the positions of the CRDCs were shifted in the dispersive plane (which affects the fragment energy). The observed location of the maximum in the decay energy spectrum changed minimally. The observed width was quite sensitive in these tests but in each test case the width increased with the artificial change. Still the quoted uncertainties for the resonance width do include a component due to this sensitivity.

IV. RESULTS AND DISCUSSION

The kinetic energy spectrum for neutrons detected in coincidence with a ^{6}He fragment is shown in Fig. 2.

The distribution is reproduced by simulation (solid line). The specific shape of the spectrum (two peaks) is related to the acceptance of MoNA. The higher energies correspond to ^{7}He decays in which the neutron was directed more forward in the center-of-mass frame while the lower energies correspond to decays in which the neutron was directed more backward. Decays in which the neutrons are emitted sideways away from the beam axis are not registered because the decay energy is large enough that the neutron will be directed outside the angular acceptance of MoNA.

The energy spectrum for the ^{6}He fragments is shown in Fig. 3.

The solid line is the result of simulation. Unlike the neutron energy spectrum, only a single peak is seen in this spectrum due to the large fragment mass resulting in smaller changes to the mean energy and the double-peak nature is not resolved. The calibration of the fragment energy was checked with beams of known energy and the neutron energy calibration (Fig. 2) was determined from γ rays from the target and a precision time calibrator. The small discrepancies between data and simulation could result from uncertainty about the production mechanism of ^{7}He in the simulation.

An important parameter for the calculation [Eq. (2)] of the decay energy is the opening angle between the neutron and the fragment. The results for this quantity are shown in Fig. 4.

The solid line is the result of simulation with parameters that best reproduce the decay energy spectrum.

The decay energy spectrum and adopted simulation result are shown in Fig. 5.

The simulation shown (solid line) is based on a resonance energy of 400(10) keV and a resonance width of $160(^{+40}_{-15})$ keV assuming that the ^{7}He ground state is an $l = 1$ state. This resonance width translates into a FWHM of $125(^{+40}_{-15})$ for the decay energy distribution (before any resolution broadening or detector acceptance cuts are applied). The FWHM is the value typically quoted in the literature. The quoted uncertainties are derived from the range of fit parameter variation and systematic uncertainty (due to uncertainties in detector positions and magnetic field strength).

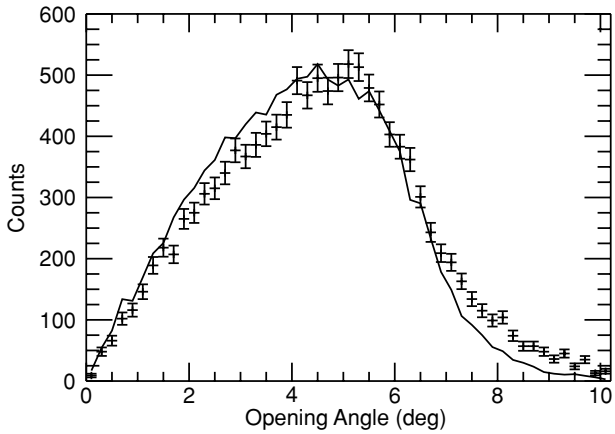

FIG. 4. The measured distribution of opening angles between the neutron and ^{6}He. The solid line is the result of simulation.

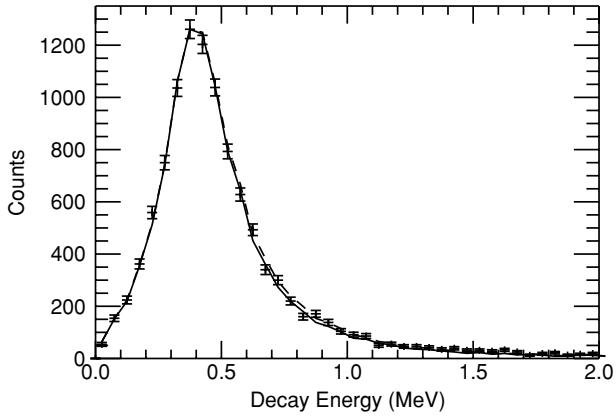

FIG. 5. The measured ^{7}He decay energy spectrum. The solid line is the result of simulation with only a single resonance (energy of 400 keV and width of 160 keV). The dashed line includes a second resonance (energy of 600 keV and width of 750 keV) [20] in the simulation.

The uncertainties also reflect the variation observed with different decay energy parametrizations and reaction models.

Although on the low side, the extracted width of $125(^{+40}_{-15})$ keV agrees well with the previous measurements and the presently adapted value of the nuclear data evaluations (150(20) keV [28]) and atomic mass evaluations (160(30) keV [29,30]). The resonance energy of 400(10) keV is apparently lower than the adapted values of 445(30) keV and 435(17) keV of the nuclear data and atomic mass evaluation, respectively. However, if one examines the individual measurements listed in Table I, our measurement agrees with every independently determined previous measurement with the exception of those reported in Ref. [17]. Most notably it agrees with the most recent and most accurate results of 430(20) keV from Ref. [20] and of 410(30) keV from Refs. [21] and [22]. Our result indicates that the resonance energy is indeed lower than the currently adapted values. These values might have been influenced by the numerous experiments quoting 440 or 450 keV based on the second measurement by Stokes and Young [2], but which did not determine the resonance independently.

The excellent fit of the decay energy shown in Fig. 5 shows that there is no evidence for an excited state. The ground state of ^{8}Li is a 2^+ state formed by coupling the $p_{3/2}$ proton with either a $p_{3/2}$ or a $p_{1/2}$ neutron. Knocking out a proton from ^{8}Li could populate either the $3/2^-$ ground state or the $1/2^-$ first excited state in ^{7}He. With the Warburton-Brown WBT p-shell Interaction [40], neutron occupations of 2.6 and 0.4 may be calculated for the $p_{3/2}$ and $p_{1/2}$ states, respectively [41]. Thus, in the reaction the first excited state of ^{7}He should at most be populated on the order of 10%.

To search for evidence for the first excited state we included such a contribution to our simulation with the resonance parameters taken from Ref. [20] as an energy of 600 keV and a width of 750 keV. The detection efficiency for the present setup decreases quickly with increasing decay energy so that it is not very sensitive to a small contribution from a state at higher energy. The contribution from this broad state is barely visible on the tail of the ground state distribution (dashed line in Fig. 5) but the reduced χ^2 increases slightly from 0.91 to 0.93. Though we found no evidence for the presence of a strong $1/2^-$ first excited state, we cannot rule it out assuming that the state is populated with less than about 20% of the strength of the ground state because of the large width of the state and the efficiency of MoNA at the resonance energy.

We note that calculations with a standard Breit-Wigner resonance shape underpredict the decay energy spectrum in the 500–800 keV region of the spectrum and would have led to an erroneous conclusion about the strength of an excited state.

V. SUMMARY AND CONCLUSIONS

The decay energy of the resonant ground state of ^{7}He has been found to be 400(10) keV with a FWHM of $125(^{+40}_{-15})$ keV. No strong evidence for other resonant states is observed. The extracted width is consistent with the published results listed in Table I and the accepted values. Although the resonance energy agrees essentially with all independently determined results, it is lower than the values quoted in the evaluations. Together with other more recent results our experiment suggests that the resonance energy of the ^{7}He ground state is lower than the currently accepted values.

ACKNOWLEDGMENTS

This work is supported by National Science Foundation Grants PHY-0606007, PHY-0651627, PHY-0555488, and PHY-0555445.

[1] R. H. Stokes and P. G. Young, Phys. Rev. Lett. **18**, 611 (1967).
[2] R. H. Stokes and P. G. Young, Phys. Rev. **178**, 2024 (1969).
[3] R. H. Lindsay, W. Toews, and J. J. Veit, Nucl. Phys. **A199**, 513 (1973).
[4] R. B. Weisenmiller, N. A. Jelley, D. Ashery, K. H. Wilcox, G. J. Wozniak, M. S. Zisman, and J. Cerny, Nucl. Phys. **A280**, 217 (1977).
[5] D. V. Aleksandrov, Yu. A. Glukhov, B. G. Novatskii, E. Yu. Nikolskii, A. A. Ogloblin, and D. N. Stepanov, Izv. Akad. Nauk SSSR Ser. Fiz. **49**, 2115 (1985).
[6] J. P. Perroud *et al.*, Nucl. Phys. **A453**, 542 (1986).
[7] C. Borcea, A. V. Belozyorov, Z. Dlouhy, A. M. Kalinin, N. H. Chau, and Yu. E. Penionzhkevich, Rev. Roum. Phys. **32**, 497 (1987).
[8] A. V. Belozerov, K. Borcha, Z. Dlougy, A. M. Kalinin, N. K. Tyau, and Yu. E. Penionzhkevich, Izv. Akad. Nauk SSSR Ser. Fiz. **52**, 100 (1988).
[9] R. A. Kryger *et al.*, Phys. Rev. C **47**, R2439 (1993).
[10] H. G. Bohlen *et al.*, Nucl. Phys. **A583**, 775 (1995).
[11] W. von Oertzen *et al.*, Nucl. Phys. **A588**, 129c (1995).

[12] M. Thoennessen *et al*., Phys. Rev. C **59**, 111 (1999).
[13] H. G. Bohlen, A. Blazevic, B. Gebauer, W. von Oertzen, S. Thummerer, R. Kalpakchieva, S. M. Grimes, and T. N. Massey, Prog. Part. Nucl. Phys. **42**, 17 (1999).
[14] A. A. Korsheninnikov *et al*., Phys. Rev. Lett. **82**, 3581 (1999).
[15] A. A. Korsheninnikov *et al*., Phys. Scr. **T88**, 199 (2000).
[16] M. S. Golovkov *et al*., Phys. At. Nucl. **64**, 1244 (2001); Yad. Fiz. **64**, 1319 (2001).
[17] L. Chen, B. Blank, B. A. Brown, M. Chartier, A. Galonsky, P. G. Hansen, and M. Thoennessen, Phys. Lett. **B505**, 21 (2001).
[18] H. G. Bohlen, R. Kalpakchieva, A. Blazevic, B. Gebauer, T. N. Massey, W. von Oertzen, and S. Thummerer, Phys. Rev. C **64**, 024312 (2001).
[19] K. Markenroth *et al*., Nucl. Phys. **A679**, 462 (2001).
[20] M. Meister *et al*., Phys. Rev. Lett. **88**, 102501 (2002).
[21] G. V. Rogachev *et al*., Phys. Rev. Lett. **92**, 232502 (2004).
[22] G. V. Rogachev *et al*., Nucl. Phys. **A746**, 229 (2004).
[23] A. H. Wuosmaa *et al*., Phys. Rev. C **72**, 061301(R) (2005).
[24] C. Nociforo, F. Cappuzzello, A. Cunsolo, A. Foti, S. E. A. Orrigo, J. S. Winfield, M. Cavallaro, S. Fortier, D. Beaumel, and H. Lenske, Eur. Phys. J. A **27**, s01, 283 (2006).
[25] N. Ryezayeva *et al*., Phys. Lett. **B639**, 623 (2006).
[26] F. Beck *et al*., Phys. Lett. **B645**, 128 (2007).
[27] F. Skaza *et al*., Phys. Rev. C **73**, 044301 (2006).
[28] D. R. Tilley, C. M. Cheves, J. L. Godwin, G. M. Hale, H. M. Hofmann, J. H. Kelley, C. G. Sheu, and H. R. Weller, Nucl. Phys. **A708**, 3 (2002).
[29] G. Audi, O. Bersillon, J. Blachot, and A. H. Wapstra, Nucl. Phys. **A729**, 3 (2003).
[30] G. Audi, A. H. Wapstra, and C. Thibault, Nucl. Phys. **A729**, 337 (2003).
[31] B. Luther *et al*., Nucl. Instrum. Methods A **505**, 33 (2003).
[32] T. Baumann *et al*., Nucl. Instrum. Methods A **543**, 517 (2005).
[33] M. D. Bird *et al*., IEEE Trans. Appl. Supercond. **15**, 1252 (2005).
[34] D. J. Morrissey, B. M. Sherrill, M. Steiner, A. Stolz, and I. Wiedenhoever, Nucl. Instrum. Methods B **204**, 90 (2003).
[35] N. Frank, Ph.D. thesis, Michigan State University, 2006.
[36] K. Makino, and M. Berz, Nucl. Instrum. Methods A **558**, 346 (2005).
[37] N. Frank, A. Schiller, D. Bazin, W. A. Peters, and M. Thoennessen, Nucl. Instrum. Methods A **580**, 1478 (2007).
[38] O. Tarasov, Nucl. Phys. **A734**, 536 (2004).
[39] A. M. Lane and R. G. Thomas, Rev. Mod. Phys. **30**, 257 (1958).
[40] E. K. Warburton and B. A. Brown, Phys. Rev. C **46**, 923 (1992).
[41] B. A. Brown (private communications).